Simulation of Stress and Strain for Induction-Hardening Applications

Dmitry Ivanov, Leif Markegård, John Inge Asperheim, and Hans Kristoffersen

The possibility to manage stress and strain in hardened parts might be beneficial for a number of induction-hardening applications. The most important of these benefits are the improvement of fatigue strength, avoidance of cracks, and minimization of distortion. An appropriate and powerful way to take the stress and strain into account during the development of a process is to make use of computer simulations. In-house developed and commercial software packages have been coupled to incorporate the electromagnetic task into the calculations. The simulations have been performed followed by analysis of the results. The influences of two different values of quenching intensity, strength of initial material structure, strength of austenite, surface power density-frequency-time combination, and workpiece diameter on the residual stress are studied. The influence of quenching intensity is confirmed by the series of experiments representing the external hardening of a cylinder with eight variations of quenching intensity. Measured by x-rays, the values of surface tangential stress are used as a dataset for verification of the model being used for analyses.

1. Introduction

The residual stress has decisive influence on the service properties of a steel component. In many cases, the compressive residual stress at the surface of a part allows for improvement of fatigue strength (both initiation and propagation crack phase), corrosion resistance, etc. (Ref 1-3).

Induction surface hardening is known as a clean, efficient, and precise process that could be integrated into a production line because of its high processing speed. Sometimes, induction surface treatment allows for improvement of fatigue life of the component regarding carburizing or shot-peening (Ref 4). Normally, the compressive stress develops at the surface of the component (Ref 5, 6). Stress levels vary in a wide range, and in some cases, the harmful tensile stress at the surface or in superficial layers can be obtained (Ref 5). A number of investigations show that the induction surface-hardening parameters have great influence on the residual stress (Ref 6-9). In order to use the results of such investigations properly, a clear understanding of the nature of influence is important. A

good explanation of the results also allows for the development of new approaches to improve the residual stress distribution.

Even simplified physics of the stress and strain development during induction hardening includes a series of nonlinear and coupled phenomena, e.g., phase transformations, heat conduction, electromagnetism, elastoplasticity, and transformation-induced plasticity (TRIP) (Ref 10, 11). Perhaps because of this, in most cases, investigators concentrate only on a couple of the important parameters that influence the residual stress. Common explanations of the compressive residual stress at the surface of an induction-hardened component are the dilatation associated with martensite formation and constraint of the relatively cold core (Ref 5, 12). Some of the investigations take additionally the plastic strain into account (Ref 8).

A common approach to analysis of the stress and strain development during induction hardening must cover the variety of the most important phenomena and reflect the internal correlations of the process. The problem of identifying such phenomena is closely related to the simulation issues. Developers of mathematical models make the assumptions and simplifications sufficient for certain predictive accuracy. The results of such investigations could be partially used for analysis of the simulation results. In this article, such an attempt is made. The constitutive relationship of a series of developed stress-strain models is used for investigation of the cause-and-effect chains in typical steel components subjected to induction surface hardening. Such relationship is the additive strain decomposition.

2. Approach to Analysis

2.1 Additive Strain Decomposition

The first step of process formalization is a choice of a sophisticated material model. The most popular metallurgic

---

Dmitry Ivanov, Leif Markegård, and **John Inge Asperheim**, EFD Induction a.s., Skien, Norway; and **Hans Kristoffersen**, Swerea IVF, Argongatan 30, 431 53 Möldal, Sweden. Contact e-mails: idg@no.efdgroup.net, lm@no.efdgroup.net, jia@no.efdgroup.net, and hans.kristoffersen@swerea.se; URL: www.efd-induction.com.

stress and strain formulations are plasticity, viscoplasticity and creep (Ref 13). Plasticity represents the rate-independent inelastic behavior of solids, whereas viscoplasticity and creep are rate-dependent phenomena. For induction hardening of steel, the plasticity model with additive decomposition of either strain or strain rate as a constitutive relationship is the most common choice because of the simplicity, and it gives sufficient accuracy (Ref 10, 11).

Regarding strain rate, strain decomposition is more preferable as an analysis instrument because the integral values of strain components could be visualized. Taking into account the features of induction-hardening processes, it can be stated for an arbitrary time of the process and point of the simulated component as follows:

$$\varepsilon_{ij} = \varepsilon_{ij}^{e} + \varepsilon_{ij}^{p} + \varepsilon_{ij}^{Th} + \varepsilon_{ij}^{Ph}, \quad \text{(Eq 1)}$$

where ε_{ij} is the total strain, ε_{ij}^{e} is the elastic strain, ε_{ij}^{p} is the plastic strain (TRIP is included), ε_{ij}^{Th} is the thermal strain, and ε_{ij}^{Ph} is the phase volumetric change strain.

Every component of strain tensor decomposition has its nature and could be interpreted from the physical point of view. The following properties of the strain components named above are important.

- Both thermal (prefix "*epsT_*"—designation on charts) and phase volumetric change ("*epsPh_*") strains are the initial sources and the cause of the effects in a hardened component. Strain has a local character and can be calculated using material properties, phase transformations, and temperature at any point of a body.
- Elastic strain ("*epse_*") directly reflects the stress. Therefore, this component must be treated with the force balance of a body taken into account. As opposed to the source strains, elastic strain cannot be considered as a local value because it reflects the part's integrity, e.g., compressive elastic strain in a hardening zone is a cause of the compensating tensile elastic strain in the core of a hardened component. Elastic strain is always limited by the yield point of the actual phase mixture for the considered moment.
- Plastic strain ("*epsp_*") is an irrecoverable part of a strain. Since the residual phase volumetric change strain is dependent on the material properties, and thermal strain is completely recoverable, plastic strain is the most important parameter that can be varied to manage the residual stress. Plastic strain can be calculated with the known laws of plastic flow, plastic criterion, etc. It is a continuation of a body reaction on the source strains, and constraints after the elastic strain is yielded.
- Total strain ("*eps_*") is an observable quantity that can be measured with known techniques. The important property of this component is a possibility to reflect the constraints of the strain. The absence of constraints makes the total strain changed with the source strains. In case the zone with acting source strains is constrained, total strain is limited in reaction and elastic strain, with a possible continuation in plastic strain takes place.

With use of the above interpretations and Eq 1, it is possible to build the cause-and-effect chains for an investigated hardened component. The tensor components could be considered separately; namely, the additive decomposition is justified also for certain directions such as axial or tangential in the cylindrical system of coordinates.

Since the main goal of this article is the analysis of residual stress, elastic strain is of main interest, and Eq 1 can be rearranged for any of the strain tensor spatial components:

$$\varepsilon^{e} = \varepsilon - \left(\varepsilon^{p} + \varepsilon^{Th} + \varepsilon^{Ph} \right). \quad \text{(Eq 2)}$$

Thermal strain depends on temperature and the coefficient of thermal expansion. Phase volumetric change strain depends on the difference between the specific volumes of initial and resulting structures. The temperature curve of the complete induction-hardening process usually is closed-loop. Therefore, the contributions of ε^{Ph} and ε^{Th} components to the residual stress value depend on the resulting structure only. With alternation of a structure's specific volume, the structure must be changed itself. This way of residual stress management is not flexible, but can be applied in practice.

According to above considerations, when a material is given, only total and plastic strains give theoretical possibility of flexible residual stress control. The difference between these values is crucial. To ensure the compressive residual stress, the plastic strain should be as high as possible, whereas the total strain should be minimized.

2.2 Geometric Considerations

At first glance, the geometric variety of hardened parts makes it impossible to apply general rules of stress development to an arbitrary region of a complex component. Indeed, the distribution of the stress is strongly dependent on the geometry of the component. Nevertheless, a big class of local regions in components could be represented as a convex or concave region. The simplest way to treat such regions is to consider them as cylindrical parts with or without an internal hole. An additional simplification and generalization of the task might be achieved by consideration of such cylinders as an infinitely long height. It is possible if the axial force balance boundary condition is imposed. In this case, the following properties of geometry should be noted (Ref 14):

- The system can be represented in a cylindrical system of coordinates. Hollow cylinder is described by two values, namely inner radius (IR) and outer radius (OR).
- There are only three nonzero spatial components of strain, namely radial (ε_r), axial (ε_z), and tangential (ε_φ) corresponding to the cylindrical system of coordinates. The postfixes "_r", "_z," and "_theta" are going to be used further to designate the spatial components on charts.

2.3 Design of Simulations

Electromagnetic and thermal tasks have been performed using software NSG ELTA. Calculation of phase transformations and stress-strain phenomena have been done by EFD Induction proprietary software based on the following models:

- Koistinen-Marburger and Avrami equations are utilized for martensitic and diffusive type transformations correspondingly (Ref 15, 16). Scheil's additivity rule is used for transition from isothermal conditions implicit in Avrami equation to continuous change of temperature (Ref 17).

- Plasticity model is based on Von Mises criterion and assumptions of isotropic hardening and associative rule of plastic flow (Ref 18).
- Leblond's model is used for incorporation of TRIP phenomenon into simulation (Ref 19).
- Finite element method is used for numerical implementation of balance equations.

In all computational cases considered in this article, calculations have been done in the following manner. First electrothermal task is calculated using NSG ELTA software. Temperature distribution for a series of time steps is exported then to EFD Induction proprietary software, and phase transformations along with stress-strain tasks are done based on imported thermal history. The considered procedure is a linear coupling of electromagnetic, thermal and phase transformation tasks. Nevertheless, the accuracy of such approach is sufficient to meet the goals of our investigation.

Design of computational experiments is represented in Table 1. The hardened surface for all the simulations except of No. 6 is external. The power and frequency of an induction heating convertor are adjusted to provide the equal austenitization depth conditions as much as possible. The maximal surface temperature after heating stage is the same for all the experiments and equal to 1000 °C. The detailed values of the variable parameters are described in corresponding sections of the article.

Material properties for steel Ck45 are used for simulations (Ref 20). Ac1 and Ac3 temperatures are corrected according to the actual heating speed (Ref 21).

3. Analysis Case

The application of the additive decomposition of the strain to analyze a real problem can be demonstrated with simulation No. 1.

The development of strain components at the external surface is shown in Fig. 1. The initial source of deformation is the thermal strain, which causes the compensating elastic and plastic strains because of the core's constraints (total strain is limited). During the austenitization, the phase volumetric change strain decreases because of the less specific volume of austenite.

After heating, the temperature at the surface starts to drop. Total strain is inert because of the adjusted layer constraints and has no possibility to react immediately. The surface is in tension, and the inversion of the elastic strain with the

continuation in plastic strain follows (Ref 8). The possibility of the plastic elongation is conditioned by the properties of the soft austenite.

Martensite formation causes an increase of the phase mixture's specific volume. This increase is the source strain that is compensated by elastic compression. Because the hardening zone suffers the compression during this stage, TRIP slightly decreases the level of accumulated plastic elongation. The above explanation can be applied to an arbitrary point of the investigated component.

4. Quenching Intensity

In a real process, the quenching intensity can be altered in a number of the different ways, namely by means of the different quenching media, spray pressure, etc. Quantitatively, this parameter is estimated with a heat-transfer coefficient (HTC) that is significantly dependent on the temperature at the cooling surface. The aim of the current investigation is to find the direction in which quenching intensity influences the results, rather than the exact residual stress distribution. Therefore,
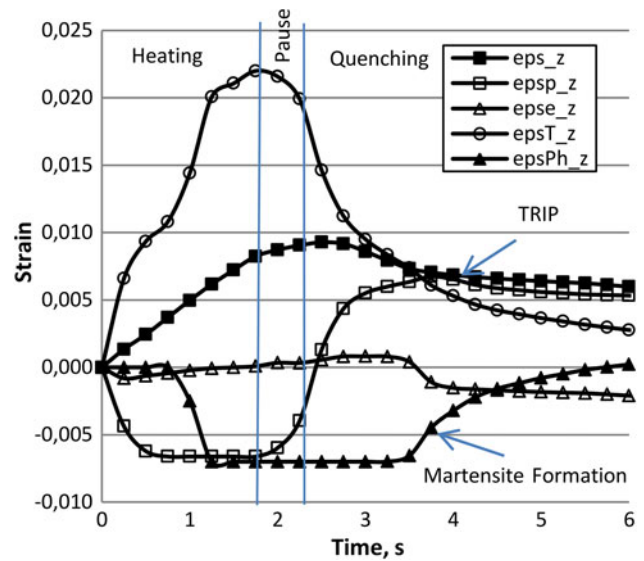

Fig. 1 Development of the strain components at the surface of a part (depth 0 mm) for simulation No. 1

Table 1 Design of simulations

Sim. No.	OR, mm	IR, mm	Current(a)/ Freq. surf. power./freq.	Heating time, s	Aus. depth(b), mm	Quench dwell, s	Variable parameter
1	10	1	2360 A/40 kHz	1.9	2.0	0.5	Reference
2	20	2	1570 A/40 kHz	2.5	2.0	0.5	External radius
3	10	1	2360 A/40 kHz	1.9	2.0	0.5	Quenching intensity
4	10	1	2360 A/40 kHz	1.9	2.0	0.5	Initial material strength
5	10	1	2360 A/40 kHz	1.9	2.0	0.5	Austenite strength
6	20	2	1530 W cm^{-2}/40 kHz	3.5	1.1	0.5	Convex/concave geometry
7	40	2	2050 A/15 kHz	2.5	2.0	0.5	External radius
8	40	2	648 A/300 kHz	8.5	2.0	0.5	Surface power density-frequency-time-combination

(a) Current in a coil of 10×10 mm Cu-conductor with core. Air gap 2 mm. (b) Austenitization temperature 840 °C

constant values of HTC have been used for an additional simplification.

Two values of HTC are considered: medium quenching intensity (MQI) for simulation No. 1 is equal to 10 kW/m^2 K, and low quenching intensity (LQI) for simulation No. 3 is equal to 5 kW/m^2 K. The distribution of the residual stress as a function of radius is shown in Fig. 2. Hereafter, prefix "*sig_*" is used for the designation of stress.

The axial compressive stress at the surface of the hardening zone for MQI simulation is about 1070 MPa, whereas for LQI, it is about 940 MPa. Tangential compressive stress is also improved for the MQI simulation. Similar results have also been obtained by other researchers (Ref 12).

The total axial strain in an infinite long cylinder is uniformly distributed. Therefore, it is more convenient to build the explanation for this direction.

The development of the axial strain components at the hardened surface for both simulations is shown in Fig. 3. At the first stage, the more intensive quenching causes a drastic decrease in the thermal strain at the surface, whereas the total strain, dependent on the average temperature of the whole cylinder, has no possibility to change so fast. As a result, plastic

elongation is prolonged for MQI (see plastic strain, 4 s). Increased resulting plastic elongation raises the residual compressive stress.

For the considered case, the increased quenching intensity plays a beneficial role. High compressive stress at the surface of a component increases the fatigue strength if crack initiation site is located at the surface.

5. Initial Structure's Strength

In the previous case, improved compressive residual stress is achieved by an increase of the plastic elongation in the hardening zone. The basic increase is attained in the time period between the end of heating and the beginning of martensite formation (plastic elongation stage). To get the same effect, strength of the initial structure can be increased. In this case, the resulting compressive plastic strain in the hardening zone after the heating stage would be reduced due to the increased elastic compensation of thermal expansion. After plastic elongation stage, the residual plastic strain level would probably be higher for this reason.

The strength of the initial structure can be improved by a pretreatment such as Q&T. In the current investigation, two cases are analysed. The first one corresponds to normalized structure of Ck45 steel (simulation No. 1). The material properties for the second case have been obtained by multiplying the temperature-dependent yield strength of the normalized structure by 2 (simulation No. 4). Abbreviations LSIS (low-strength initial structure) and HSIS (high-strength initial structure) are used. Temperature dependencies of the yield limit for both simulations are shown in Table 2.

The comparison of the residual stress for these cases is shown in Fig. 4. Indeed, a small improvement of the compressive stress in the hardening zone can be observed for the
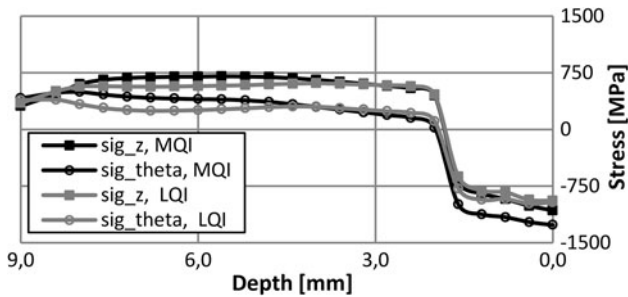

Fig. 2 Residual stress for the different quenching intensities
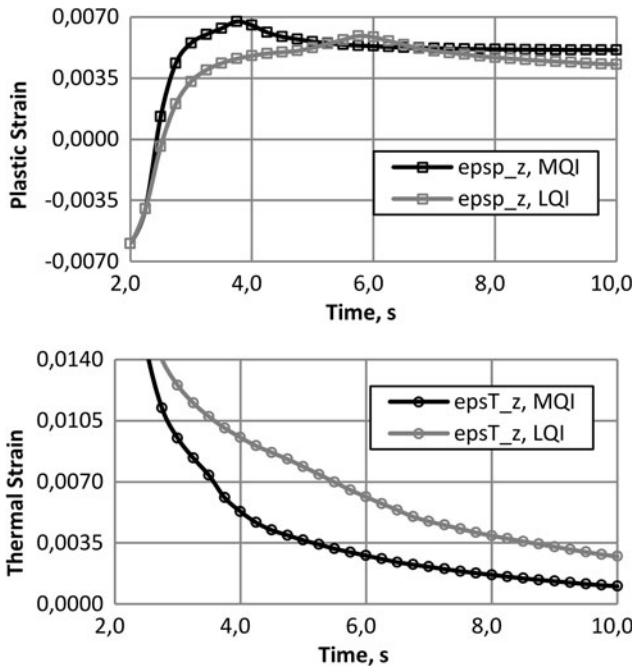

Fig. 3 Development of axial strain at the surface of the part during quenching for the different quenching intensities

HSIS-case. Another important factor for the HSIS case is an increase of the detrimental tensile stress at the core's border. Such behavior has been already revealed by the experimental investigations (Ref 7).

Thermal and phase transformation conditions are equal for both simulations. Therefore, the examination of the development of total and plastic strains is enough for explanation (Fig. 5).

The comparison of total strain developments during heating shows greater constraints for the surface in case of HSIS. Since the thermal and phase transformation conditions are the same, the elastic and plastic strains are responsible for this behavior of the total strain. During heating, compressive stress in the heating zone is compensated by tensile stress in the central part of the core. HSIS allows higher stress (elastic strain). In the case of LSIS, the elastic strain is rapidly yielded and continued in a plastic elongation of the core.

The described process is shown in Fig. 6 with the distribution of the plastic strain just before quenching. The core's elongation weakens the constraint for the hardening zone. As can be seen in Fig. 6, the plastic compression at the surface is lower for LSIS before quenching.

After the quenching has begun, the core's border, as well as the hardening zone, is subjected to thermal contraction that requires compensation according to Eq 1.

Table 2 Yield limit of initial structure

Temperature, °C	20	400	800
LSIS yield limit, MPa	335	55	10
HSIS yield limit, MPa	670	110	20
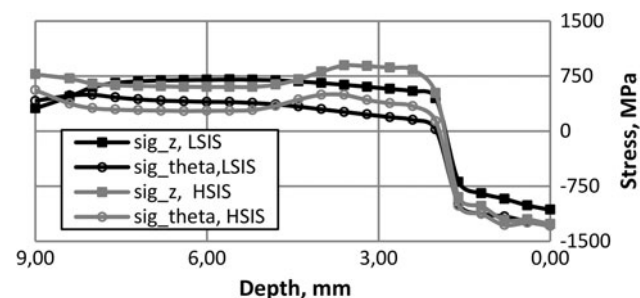
Fig. 4 Distribution of residual stress for the different strengths of the initial structure
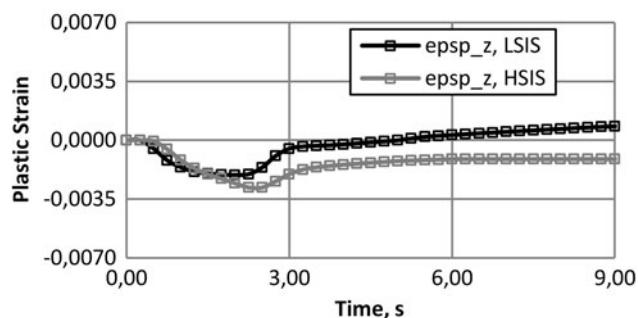
For both the HSIS and LSIS cases, such compensation is again a reaction of the plastic and elastic strains, but because of a high yield limit of the core, the plastic elongation for HSIS is less compared with LSIS. At the same time, the hardening zone has the same austenite properties. As a result, the residual stress in the hardening zone is improved, but the core's border suffers the high detrimental tensile stress.

6. Austenite Strength

Strength of austenite depends on the different factors such as a temperature, austenite's homogeneity and grain size, the presence of the undissolved carbides in the austenite's matrix, etc. Since the yield limit of a material influences the relation between the elastic and plastic strains, it is hypothetically possible to achieve a greater plastic elongation magnitude for the cases of weak austenite. To verify this assumption, the austenite properties of Ck45 steel are modified by a simple multiplication of the temperature-dependent yield strength by 2. The abbreviation LSA (low-strength austenite) is given to the reference simulation No. 1, and HSA (high-strength austenite) for simulation No. 5 with modified austenite properties. The temperature dependencies of the yield limit of austenite for both experiments are shown in Table 3.

Distribution of the residual stress is quite unexpected. With a sufficient accuracy, residual stresses for LSA and HSA are equal (Fig. 7). The same result has been achieved for other geometries and austenite properties.

To understand the cause of such stress behavior, we can investigate the strain development curves in depth 1 mm (Fig. 8). The stress evolution can be evaluated with elastic strain, whereas change volumetric strain can be used for identification of certain transformation moments.

Difference in stress for hot austenite is negligible because of the small level of yield limit (see Table 3).

The temperature drops after 1.9 s of heating, and this causes the plastic elongation for both cases according to explanation in section 4. Cooling of the austenite zone leads to an increase of the yield limit difference and, therefore, the difference in plastic and elastic strain relations. As a result, stress is higher and plastic elongation is lower for HSA case. The stress difference is at a maximum just before martensite formation. This fact is in good agreement with the initial considerations of this section. However, immediately after the martensite formation has started, the plastic strain in HSA case starts to grow
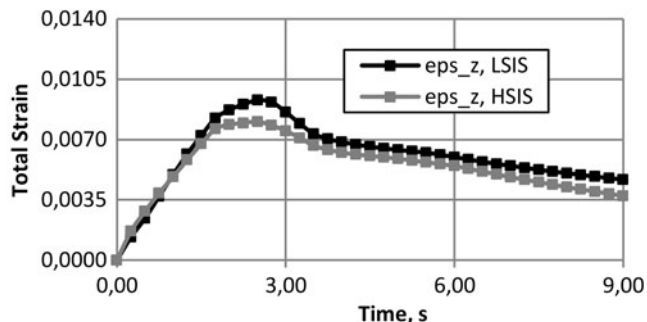
Fig. 5 The development of the plastic and total strains at the border of a core (depth 2.6 mm) for the different initial structures
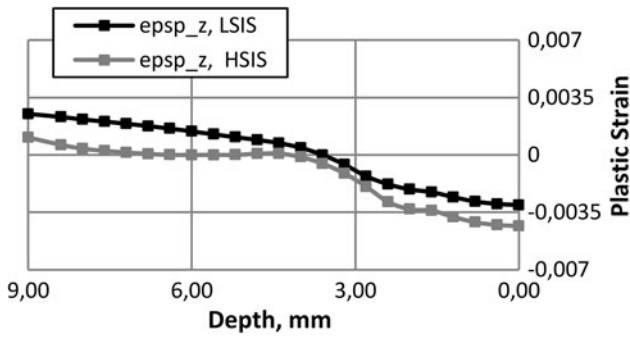
Fig. 6 Axial plastic strain distribution just before quenching (time 2.4 s)

Table 3 Yield limit of austenite

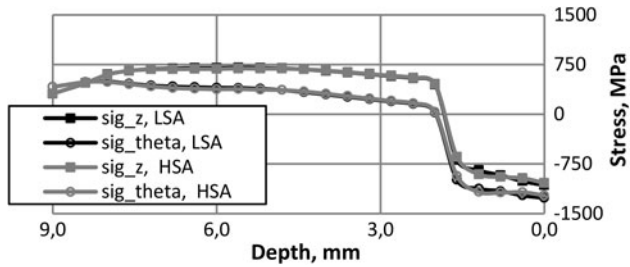| Temperature, °C	20	400	900
LSA Yield limit, MPa	243	39	7
HSA Yield limit, MPa	486	78	14

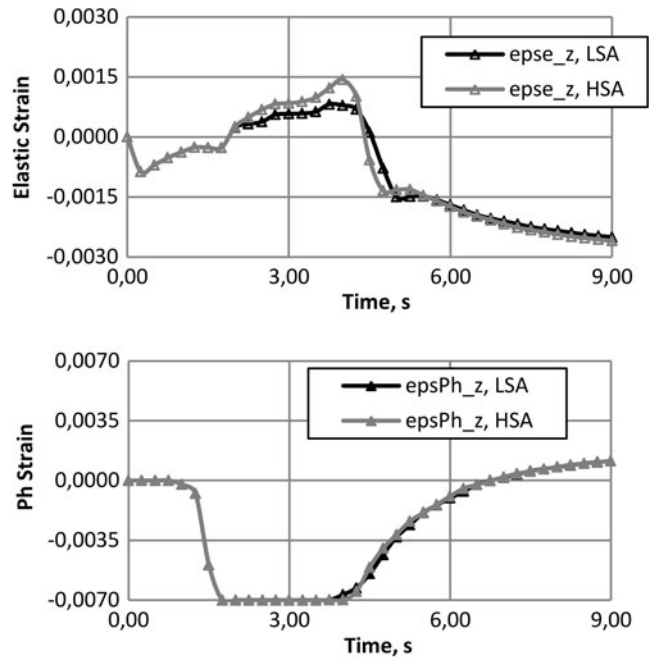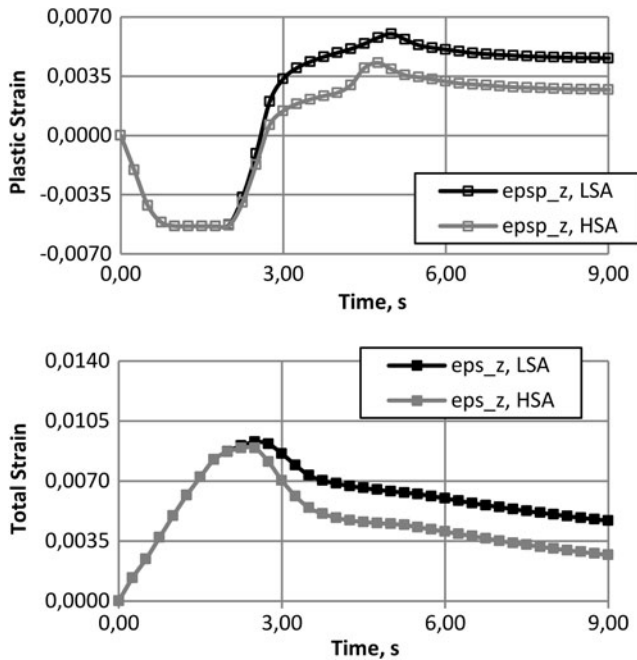**Fig. 7** Residual stress distribution for the different austenite's strength

significantly. The difference in elastic strain then quickly becomes negligible.

At first glance, such behavior of plastic strain in HSA case is strange. Indeed, the austenite matrix starts to strengthen by martensite, and plastic flow gets into difficulties. Another aspect of plastic flow in steels must be responsible for this, namely the TRIP phenomenon. Relatively high tensile stress during the early martensite formation in HSA case introduces the additional plastic strain increment into total elongation when the plastic flow in a common sense is impossible.

As it was already stated in section 2.1, the difference between the total and plastic strains is crucial for residual stress in condition of equal thermal and phase volumetric change strains. The TRIP effect makes these differences equal in the two cases.

It can be concluded that the austenite yield limit does not influence the residual stress itself. Distortion-related problem can be observed, namely, the difference in total strain.

7. Part Outside Diameter

The geometric factor has a great influence on the development of the stress and strain in a component. Three different cases have been investigated.

Simulation No. 1 represents a small outside diameter (SOD), and simulations No. 2 and No. 7 are for the medium and large outside diameters (LOD), respectively.

The result of simulations is presented in Fig. 9. It can be concluded that with a reduced outside diameter, compressive stress in a hardening zone is improved. The explanation can be built on the comparison of SOD and LOD simulations (Fig. 10).

According to the total strain curve, the hardening zone during heating for SOD simulation is weak-constrained as

Fig. 8 Development of axial strains in hardening zone (depth 1 mm) for the different austenite's strength

opposed to LOD. As a result, the plastic contraction during heating is less, and the residual plastic elongation is greater for SOD.

The decreasing of constraints for small diameters is ascribed to smaller differences in the temperature inside a part due to heat conduction. The whole core is heated and expanded more due to its higher average temperature, thereby enabling the hardening zone to expand more easily.

8. Convex Versus Concave Geometries

To compare the hardening of the convex and concave geometries, we can compare simulation No. 2 (external hardening) and simulation No. 6, in which the internal

hardening (IH) is performed. Distributions of the residual plastic strain and stress are shown in Fig. 11.

The most important result is the tangential tensile residual stress for IH case. The magnitude of the tangential residual plastic strain differs by ten times and is in contraction. Such "tangential anomaly" occurs when the heated zone is stiffly constrained by a relatively cold core (large OD) and the expansion has to go into the bore when the radius decreases. This process can be observed in Fig. 12.

Total strain at the surface for IH case is negative despite the occurrence of thermal expansion during the heating stage. Such "over-constraint" causes the great plastic compression.

The effect of "anomaly" is magnified by small ID. It can be seen that this effect could be very harmful for the residual stress.

The large difference in the axial components of plastic strain can be explained by the thermal conduction in a cylindrical system. Heating the core through a small internal diameter is more difficult compared with the external heating. Therefore, the surface power density for simulation No. 6 is increased significantly. The constraints of the core in these conditions are stiffer, since its average temperature is low. Hence, a greater plastic contraction during the heating stage develops for the IH case, and the residual plastic elongation has a smaller magnitude.
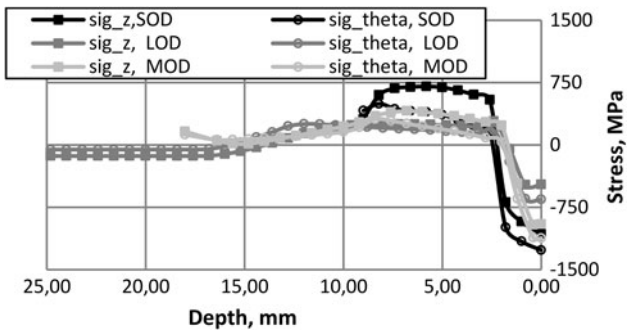
9. Induction Heating Parameters

A distinctive characteristic of induction heating is the possibility to generate heat sources not only at the surface, but

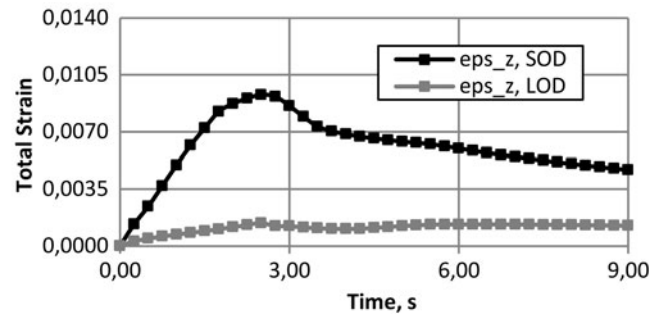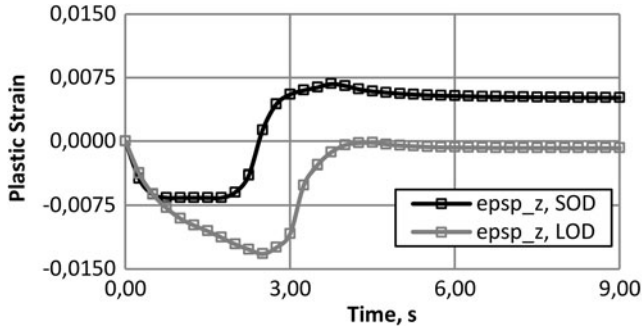**Fig. 9** Residual stress for the different outside diameters of a part

Fig. 10 The development of axial strains at the surface of a part for the different part outside diameters
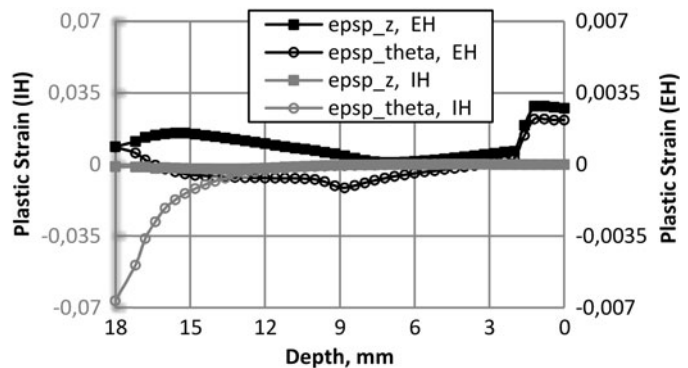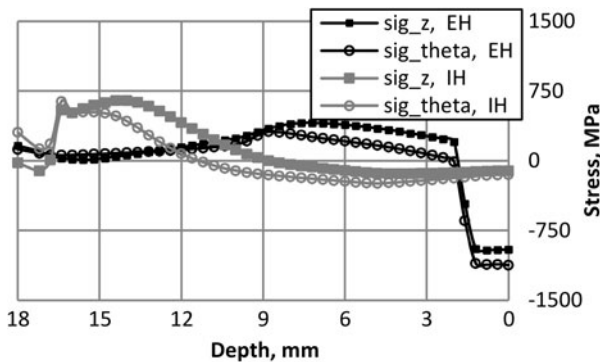

Fig. 11 Residual stress and plastic strain for external and internal hardening of hollow cylindrical part

also at a certain depth. The distribution of heat sources depends on converter frequency, power, geometric parameters of "induction coil and hardened part" system, and steel properties (Ref 22). Since the latter parameter depends on temperature, the distribution of the heat sources varies during the heating process. Selection of the induction-heating process parameters is described in the specialized literature (Ref 23).

In case of a specified power generated in an induction coil, the volume power density in the superficial layers will increase with frequency. To avoid overheating the surface and get the same hardening depth, the power should be reduced and the heating time increased with a higher frequency. Beside this, the thermal properties of steel and dimensions of a part should be taken into account to ensure the equal austenitization conditions for the different heating frequencies (Ref 22). Therefore, it is justified to consider a set of parameters "frequency-surface power density-heating time" for any specified system of "induction coil and hardened part" and required austeninization depth. The

possibility to choose between such sets presents a question: Which set is better from the residual stress point of view?

In the current study, two different combinations of surface power density, frequency, and time are used for comparison. First combination is based on the 15 kHz frequency and a heating time of 2.5 s (simulation No. 7). The second one is adjusted to get the same austenitization conditions with a high frequency of 300 kHz and a heating time of 8.5 s (simulation No. 8). The abbreviations MFH (medium-frequency heating) and HFH (high-frequency heating), are used respectively.

The residual distributions of stress and plastic strain are shown in Fig. 13.

The compressive stress is increased significantly for HFH case. As can be seen in the plastic strain distribution, the cause of such stress improvement is the prolonged plastic elongation both for axial and tangential spatial components.

The development of axial plastic and total strain at the hardened surface is built to understand the nature of increased
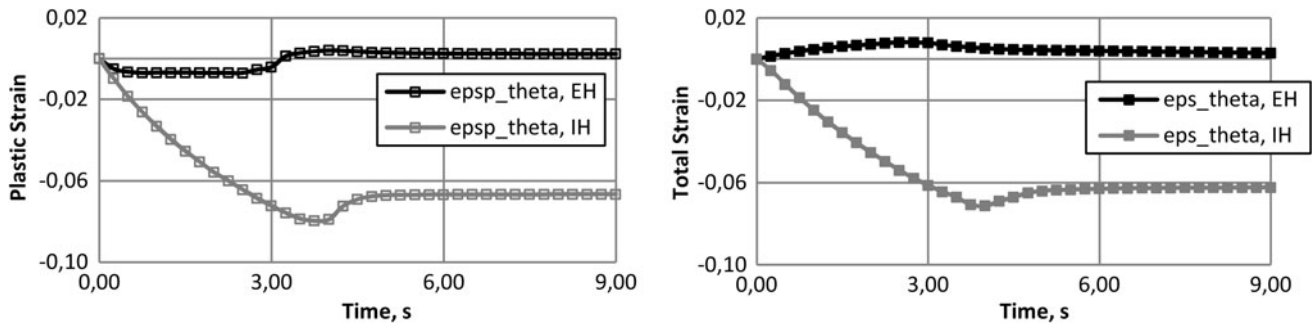

Fig. 12   The development of tangential strains at the surface of a part for external and internal hardening of hollow cylindrical part
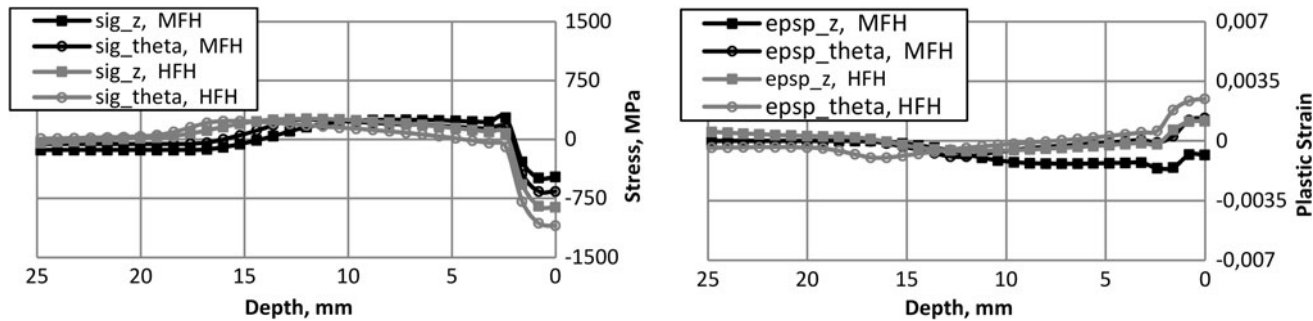

Fig. 13   Residual stress and plastic strain for the two surface power density-frequency-time combinations
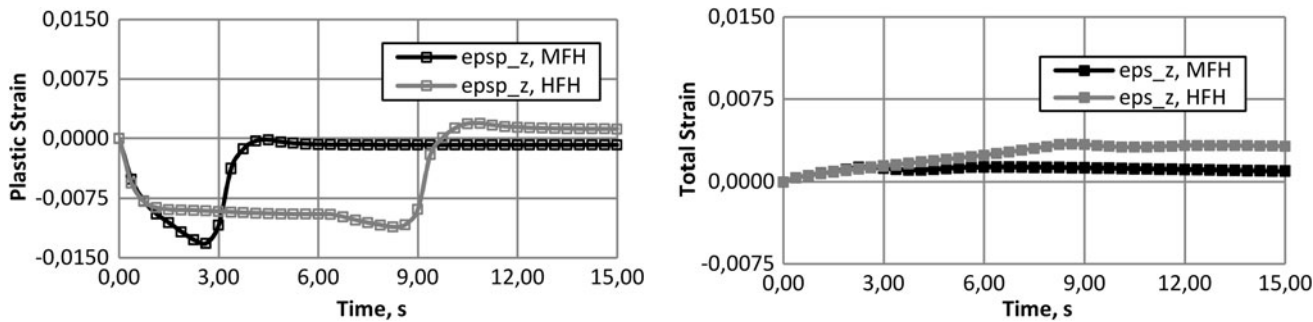

Fig. 14   The development of axial strains at the surface of a part for the different surface power density-frequency-time combinations

magnitude of plastic elongation (Fig. 14). It can be clearly seen that the total strain in HFH case is increased. It means that the hardening zone for this case is less constrained by core, and because of that plastic compression on the heating stage is deceased.

The resulting plastic elongation is higher for HFH case because of the expanded core due to the longer heating time. The cause of such expansion is the higher average temperature of the core. The distribution of thermal strain just before quenching for both simulations is shown in Fig. 15. It can be clearly seen that thermal expansion of the hardening zones are almost equal, whereas the difference in the core average temperatures is significant. Heating time for HFH case is much longer, and the temperature is more uniformly distributed along the radius because of the heat conduction.

The described principle of compressive residual stress increase is related to one explained in section 7. In both cases, the responsible cause for the increased plastic elongation is the higher average core temperature.

10. Experimental Verification

As was shown by the simulations, quenching intensity influences the residual stress distribution. The constant values of HTC have been used to find the direction of influence in case of convex geometry being hardened. In order to confirm the obtained result in case of actual quenching conditions, a set of experiments has been undertaken in collaboration with Swerea IVF, Sweden. Steel C45 solid bar with diameter of 20 mm and
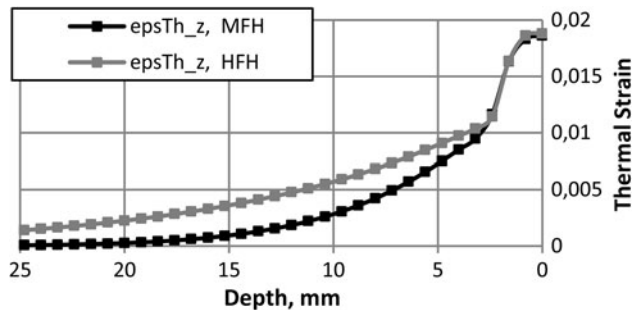
height of 50 mm was subjected to induction-hardening process with the following parameters:

- Induction heating frequency: 25 kHz;
- Heating time: 3 s;
- Maximum surface temperature: 930 °C;
- Dwell time before quenching: 1 s;
- Quenching time: 15 s.

For full factorial design of the experiment, varying three quenching parameters at two levels has been accepted. The variable parameters are concentration of polymer in fresh water, temperature of quenchant, and flow rate.
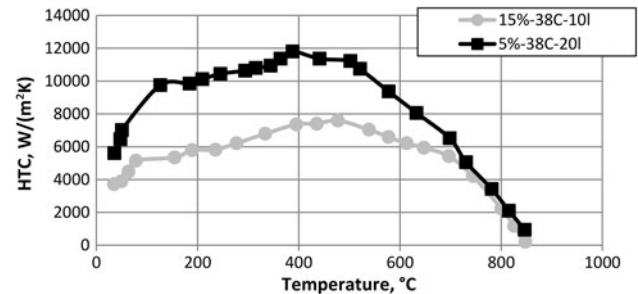
Fig. 16 HTCs for the slowest and fastest quenching intensities used in simulations
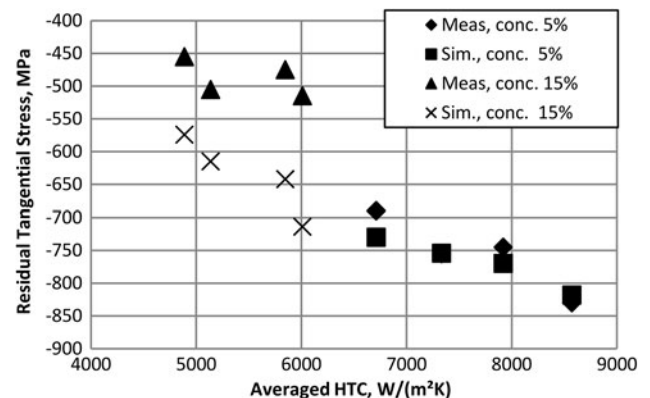
Fig. 17 Measured and simulated residual tangential stress depending on averaged HTC

Fig. 15 Axial thermal strain distribution just before quenching for the different surface power density-frequency-time combinations (time 3 s for MFH, 9 s for HFH)

Table 4 Results of experiments and simulations

Exp. no.	Concentration, %	Temperature, °C	Averaged HTC, W/(m² K)	Flow rate, L/min	Meas. sig_theta at surface, MPa	Sim. sig_theta at surface, MPa	Absolute error, MPa
1	5	22	8571	20	−830	−818	12
2	5	22	7332	10	−755	−754	1
3	5	38	7921	20	−745	−770	−25
4	5	38	6712	10	−690	−730	−40
5	15	22	6010	20	−515	−714	−199
6	15	22	5137	10	−505	−615	−110
7	15	38	5848	20	−475	−642	−167
8	15	38	4890	10	−455	−574	−119

The tangential residual stress was measured at a depth of 0.045 mm below the surface using x-ray-unit Xstress 3000 (Stresstech) with a collimator size of 1 mm. The estimated experimental error is of ±25 MPa.

In order to verify models being used, the design of experiments was replicated through simulations. HTC dependencies on temperature obtained with the help of *ivf Smart-Quench* system and software *SQIntegra* have been imposed as boundary conditions at a quenching stage. HTCs for the factor combinations that give the fastest (exp. no. 1, Table 4) and the slowest cooling rates (exp. no. 8, Table 4) are shown in Fig. 16.

The results of experimental measurements and simulations are represented in Table 4 and Fig. 17. HTC values are represented as an average value. A good conformity between model and measurements can be seen for the cases of the low polymer concentration of 5%. The worst absolute error in this case is only of −40 MPa. Polymer concentration of 5% corresponds to higher average values of HTC.

In the case of 15% polymer concentration, the predictions of model systematically give more compressive stress than those measured. This is shown in Fig. 16. The plausible explanation of this discrepancy is the difference in microstructure along the hardening zone due to insufficient quenching intensity. Such a difference is not taken into account in the model, and the volumetric change of martensite is considered as equal for two equal portions of martensite. In addition, the phenomenon known as auto-tempering and associated decrease in volumetric strain in superficial hardened layers can contribute the observed result.

Experiments and simulations show a general trend toward a beneficial influence of intensive quenching on compressive residual stress in convex hardened components. Moreover, the insufficient quenching can result in an even higher loss in compressive stress than that predicted by a simple model because of the microstructural effects.

11. Conclusions

The additive decomposition of strain is a convenient instrument for analysis of different stress and strain effects in an induction-hardened steel part. Examination of the development of the strain component allows taking into account a wide range of cause-and-effect relations. The proposed explanations are based on calculation results from approved and verified mathematical models.

Simulations have shown the important role that the plastic and total strains play on residual stress formation. Understanding the behavior of strain's development allows for changes in the induction surface-hardening parameters to get the best result.

Benefits of high average temperature of the core are demonstrated. Intensive quenching allows keeping the core's temperature at a relatively high level until the end of martensite transformation in the hardening zone. At the same time, a disadvantage of intensive quenching can be the crack initiation during a quenching process (Ref 24). Therefore, the use of high quenching intensity should be handled with care. A smaller outer diameter gives increased average core temperature due to heat conduction in the part. The same nature of the compressive residual stress improvement can be observed in case of longer heating with use of higher frequencies.

The influence of initial material strength is more complicated. A high level of tensile stress can be achieved at the core's border for the strengthened initial structure.

Changes in austenite's yield limit have negligible effect on the distribution of residual stress. Simulations reveal that this is due to the TRIP effect. Since the proper incorporation of TRIP into calculations is an open problem, it is difficult to estimate the relevance of this result to real cases. Despite the lack of difference in residual stress, the residual difference in total strain can be observed for the distinct austenite yield limit.

A big difference between the hardening of convex and concave geometries is demonstrated. In case of IH (concave geometry), the "tangential anomaly" is of great interest because of the detrimental effect it has on the residual stress.

The model being used for simulations is verified by the series of experiments. The acceptable conformity of simulations and measurements has been found. Besides, the influence of quenching intensity on residual stress at the surface of a convex-hardened component is confirmed by experiments.

References

1. J. Lu, Prestress Engineering of Structural Material: A Global Design Approach to the Residual Stress Problem, *Handbook of Residual Stress and Deformation of Steel*, M. Howes, T. Inoue, and G. Totten, Ed., ASM International, Materials Park, OH, 2001, p 11–26
2. D. Löhe, K.-H. Lang, and O. Vöhringer, Residual Stress and Fatigue Behavior, *Handbook of Residual Stress and Deformation of Steel*, G. Totten, M. Howes, and T. Inoue, Ed., ASM International, Materials Park, OH, 2001, p 27–53
3. G.A. Webster and A.N. Ezeilo, Residual Stress Distributions and Their Influence on Fatigue Lifetimes, *Int. J. Fatigue*, 2001, **23**, p S375–S383
4. D. Coupard, T. Palin-Iuc, P. Bristiel, V. Ji, and C. Dumas, Residual Stresses in Surface Induction Hardening of Steels: Comparison Between Experiment and Simulation, *Mater. Sci. Eng.*, 2008, **A**(487), p 328–339
5. Z. Li, A. Freborg, and B.L. Ferguson, Applications of Modeling to Heat Treat Processes, *Heat Treat. Prog.*, 2008, **8**, p 28–33
6. J. Grum, Induction Hardening, *Handbook of Residual Stress and Deformation of Steel*, G. Totten, M. Howes, and T. Inoue, Ed., ASM International, Materials Park, OH, 2001, p 220–247
7. H. Kristoffersen and P. Vomacka, Influence of Process Parameters for Induction Hardening on Residual Stress, *Mater. Des.*, 2001, **22**, p 637–644
8. L. Markegård and H. Kristoffersen, Residual Stress after Surface Hardening—Explanation of How Residual Stress is Created, *Dubrovnik 2009*, 2009, pp. 359–366
9. S. Hossain, C.E. Truman, D.J. Smith, and M.R. Daymond, Application of Quenching to Create Highly Triaxial Residual Stress in Type 316H Stainless Steel, *Int. J. Mech. Sci.*, 2006, **48**, p 235–243
10. D. Hoemberg, A Mathematical Model for Induction Hardening Including Mechanical Effects, *Nonlinear Anal. Real World Appl.*, 2004, **5**, p 55–90
11. C. Şimşir and C.H. Gür, A Mathematical Framework for Simulation of Thermal Processing of Materials: Application to Steel Quenching, *Turkish J. Eng. Environ. Sci.*, 2008, **32**, p 85–100
12. N. Kobasko, Optimal Quenched Layer at the Surface of Steel Parts, *Dubrovnik 2001*, 2001, pp. 25–33
13. H. Alberg and D. Berglund, Comparison of Plastic, Viscoplastic, and Creep Models when Modeling Welding and Stress Relief Heat Treatment, *Comput. Methods Appl. Mech. Eng.*, 2003, **192**, p 5189–5208
14. B.A. Boley and J.H. Weiner, *Theory of Thermal Stresses*, Dover, New York, 1997
15. M. Avrami, Kinetics of phase change. I. General theory, *Chem. Phys.*, 1939, **8**, p 565–567
16. D.P. Koistinen and R.T. Marburger, A General Equation Prescribing the Extent of the Austenite-Martensite Transformation in Pure Iron-Carbon Alloys and Plain Carbon Steels, *Acta Metall.*, 1959, **7**, p 59–60

17. E. Scheil, Anlaufzeit Der Austenitumwandlung, *Arch. Eisenhuttenwes.*, 1935, **8**, p 565–567

18. J. Chakrabarty, *Theory of Plasticity*, Elsevier Butterworth-Heinemann, Oxford, 2006

19. J.B. Leblond, Mathematical Modeling of Transformation Plasticity in Steels II. Coupling with Strain Hardening Phenomena, *Int. J. Plast.*, 1989, **5**, p 573–591

20. H.J.M. Geijselaers, Numerical Simulation of Stresses due to Solid State Transformations, *The Simulation of Laser Hardening*, Ponsen & Looijen, Hellendoorn, Thesis University of Twente, Enschede, 2003, p. 142 (with ref. with Summary in Dutch)

21. J. Orlich, A. Nose, and P. West, *Atlas zur Warmebehandlung der Stahle*, M.B.H., Dusseldorf, 1973

22. L. Markegård and J.I. Asperheim, New Nomographs for Induction Surface Hardening of Steel, *Dresden 2003*, 2003

23. S.L. Semiatin and D.E. Stutz, *Induction Heat Treatment of Steel*, ASM International, Materials Park, OH, 1986

24. N.I. Kobasko, V.S. Morganyuk, and V.V. Dobrivecher, Control of Residual Stress Formation and Steel Deformation during Rapid Heating and Cooling, *Handbook of Residual Stress and Deformation of Steel*, G. Totten, M. Howes, and T. Inoue, Ed., ASM International, Materials Park, OH, 2001, p 312–330